Disappearance of Hard X-Ray Emission in the Last BeppoSAX Observation of the Z Source GX 349+2

Iaria, R.; di Salvo, T.; Robba, N.R.; Burderi, L.; Stella, L.; Frontera, F.; van der Klis, M.B.M.

Published in:
Astrophysical Journal

DOI:
10.1086/379645

The Astrophysical Journal, 600:358–367, 2004 January 1

DISAPPEARANCE OF HARD X-RAY EMISSION IN THE LAST *BeppoSAX* OBSERVATION OF THE Z SOURCE GX 349+2

R. Iaria,[1] T. Di Salvo,[1,2] N. R. Robba,[1] L. Burderi,[3] L. Stella,[3] F. Frontera,[4,5] and M. van der Klis[2]
Received 2003 April 30; accepted 2003 August 4

ABSTRACT

We report on the results from two *BeppoSAX* observations of the Z source GX 349+2 performed in 2001 February and covering the broad energy range 0.12–200 keV. The light curve obtained from these observations shows a large flaring activity, the count rate varying from ~130 to ~260 counts s^{-1}, indicating that the source was in the flaring branch during these observations. The average spectrum is well described by a soft blackbody ($kT_{\rm BB} \sim 0.5$ keV) and a Comptonized component having a seed photon temperature of $kT_0 \sim 1$ keV, an electron temperature of $kT_e \sim 2.7$ keV, and optical depth of $\tau \sim 11$. To well fit the energy spectrum, three Gaussian lines are needed at 1.2, 2.6, and 6.7 keV with corresponding equivalent widths of 13, 10, and 39 eV, probably associated to L-shell emission of Fe xxiv, Lyα S xvi, and Fe xxv, respectively. These lines may be produced at different distances from the neutron star, which increase when the count rate of the source increases. An absorption edge is also needed at 9 keV with an optical depth of $\sim 3 \times 10^{-2}$. From the color-color diagram (CD), we selected five zones from which we extracted the corresponding energy spectra. The temperatures of the blackbody and of the Comptonized component tend to increase when the intensity of the source increases. We discuss our results comparing them to those obtained from a previous *BeppoSAX* observation, performed in 2000 March, during which the source was in a similar position on its Z-track. In particular, we find that, although the source showed similar spectral states in the 2000 and the 2001 observations, a hard tail that was significantly detected in 2000 March is not observed in these recent observations.

Subject headings: accretion, accretion disks — stars: individual (GX 349+2) — stars: neutron — X-rays: binaries — X-rays: general — X-rays: stars

1. INTRODUCTION

Low-mass X-ray binaries (LMXBs) containing old and low magnetic-field neutron stars (NSs) are usually divided into Z and atoll sources, according to the path they describe in an X-ray color-color diagram (CD) or hardness-intensity diagram (Hasinger & van der Klis 1989) assembled by using the source count rate over a typical (usually 2–20 keV) X-ray energy range. Atoll sources are usually characterized by relatively low luminosities (~0.01 – 0.2 $L_{\rm Edd}$) and some show transient behavior, while the six known Z sources in the Galaxy are among the most luminous LMXBs, accreting persistently close to the Eddington limit ($L_{\rm Edd}$) for a 1.4 $M_\odot$ NS. The instantaneous position of an individual source in the CD, which determines most of the observed spectral and temporal properties of the source, is thought to be an indicator of the mass accretion rate (e.g., Hasinger et al. 1990; see van der Klis 1995 for a review). It has been suggested that the mass accretion rate (but not necessarily the X-ray luminosity) of individual sources increases along the track from the top left to the bottom right, i.e., from the islands to the banana branch in atoll sources and from the horizontal branch (HB) to the normal branch (NB) and to the flaring branch (FB) in Z sources.

However, while there is a general correlation between temporal variability properties (in particular, frequencies of the observed quasi-periodic oscillations [QPOs]; see van der Klis 2000 for a review) and position in the CD, the correlation with the source X-ray count rate or X-ray flux in the 2–50 keV energy range is complex; a correlation is observed on short timescales (hours to days) but not on longer timescales. A possible explanation of this behavior is that most timing and spectral parameters are determined by the dynamical properties of the accretion disk, while the X-ray flux is determined by the total accretion rate, which may be different from the instantaneous accretion rate through the disk if, for instance, matter can flow radially close to the NS (see, e.g., van der Klis 2001).

Hard X-ray spectra extending up to energies of several tens to a hundred keV have been revealed in about 20 "faint" NS LMXBs (some of them are confirmed atoll sources; see Di Salvo & Stella 2002 for a review). In these systems, a power-law–like component is observed, with typical photon indices of ~1.5–2.5 and a high-energy exponential cutoff between ~20 and many tens of keV. This component is interpreted in terms of unsaturated thermal Comptonization. Sometimes, in the so-called hard state of atoll sources, there is no evidence for a cutoff up to ~100–200 keV. Some sources appear to spend most of the time in this state (e.g., 4U 0614+091; Ford et al. 1996; Piraino et al. 1999 and references therein). In others, a gradual transition from the soft to the hard state has been observed in response to a decrease of the source X-ray luminosity and/or the source drifting from the banana branch to the island state. This transition is often modeled in terms of

[1] Dipartimento di Scienze Fisiche ed Astronomiche, Università di Palermo, via Archirafi 36, 90123 Palermo, Italy; iaria@gifco.fisica.unipa.it.
[2] Astronomical Institute Anton Pannekoek, University of Amsterdam and Center for High-Energy Astrophysics, Kruislaan 403, NL 1098 SJ Amsterdam, Netherlands; disalvo@science.uva.nl.
[3] Osservatorio Astronomico di Roma, Via Frascati 33, 00040 Monteporzio Catone, Rome, Italy.
[4] Physics Department, University of Ferrara, Via Paradiso 12, 44100 Ferrara, Italy.
[5] IASF-CNR Section of Bologna, Via P. Gobetti 101, 40129 Bologna, Italy.

a gradual decrease of the electron temperature (and increase of the optical depth) of the Comptonizing region.

On the other hand, the spectrum of the Z sources is much softer, with cutoff energies usually well below 10 keV. However, hard tails were occasionally detected in their spectra. A variable hard component dominating the spectrum of Sco X-1 above ~40 keV was detected as early as 1966 (Peterson & Jacobsen 1966; see also Riegler, Boldt, & Serlemtsos 1970; Agrawal et al. 1971; Haymes et al. 1972). In other occasions, the hard tail in Sco X-1 was not found (e.g., Miyamoto & Matsuoka 1977 and references therein; Soong & Rothschild 1983; Jain et al. 1984; Ubertini et al. 1992), perhaps owing to pronounced variations. Evidence for a hard component was also found in Cyg X-2 (Peterson 1973), GX 349+2 (Greenhill et al. 1979) and in *Ginga* data of GX 5-1 (although, in this case, a contribution from a contaminating source could not be excluded; Asai et al. 1994).

Renewed interest in the hard X-ray emission properties of luminous LMXBs was motivated by some recent observations, mostly using the broadband capabilities of *BeppoSAX* (0.1–200 keV) and *RXTE* (2–220 keV). Recently, a hard tail was detected in GX 17+2, observed by *BeppoSAX*. In this case, the intensity variations of the hard tail were clearly correlated with the source spectral state: a factor of 20 decrease was observed in moving from the HB to the NB (Di Salvo et al. 2000). The presence of a variable hard tail in Sco X-1 was recently confirmed by OSSE and *RXTE* observations (Strickman & Barret 2000; D'Amico et al. 2001). A hard tail was also detected in GX 349+2 (Di Salvo et al. 2001, hereafter Paper I) and Cyg X-2 (Frontera et al. 1998; Di Salvo et al. 2002) as well as in the peculiar bright LMXB Cir X-1 (Iaria et al. 2001). These hard components can be fitted by a power law, with a photon index in the range 1.9–3.3, contributing up to 10% of the total source luminosity.

GX 349+2, also known as Sco X-2, was called an oddball among the Z sources (Kuulkers & van der Klis 1998). Similar to the case of Sco X-1, GX 349+2 shows a short and underdeveloped HB (if at all). The source variability in the frequency range below 100 Hz is closely correlated with the source position on the X-ray CD, as in other Z sources. Quasi-periodic oscillations at kHz frequencies (kHz QPOs) were detected in the NB of its Z track (Zhang, Strohmayer, & Swank 1998). However, GX 349+2, which sometimes shows broad noise components changing not only with the position in the Z but also as a function of the position in the hardness-intensity diagram, differs somewhat from the other Z sources and shows similarities to the behavior seen in bright atoll sources such as GX 13+1 and GX 3+1 (Kuulkers & van der Klis 1995; see also O'Neill et al. 2001, 2002). Using a *BeppoSAX* observation performed in 2000 March, Di Salvo et al. (2001) showed that the source energy spectrum below 30 keV could be well fitted by a blackbody (with a temperature of 0.5–0.6 keV) and a Comptonized component (with a seed-photon temperature of ~1 keV and an electron temperature of ~2.7 keV). Three discrete features were observed in the spectrum: an emission line at 1.2 keV, probably associated to Ne X or a complex L shell of Fe XXIV, an emission line at 6.7 keV and an absorption edge at 8.5 keV, both corresponding to emission from the K shell of highly ionized iron (Fe XXV). Above 30 keV, during the nonflaring state, a power-law component was significantly detected having a photon index of ~ 1.9 and a flux of $\sim 1.2 \times 10^{-10}$ ergs cm^{-2} s^{-1} in the energy band 10–60 keV. Because there was no evidence of contaminating sources, the authors concluded that the most probable candidate for the hard emission was GX 349+2 itself. The hard component detected in GX 349+2 is one of the hardest among the high-energy components detected so far in bright LMXBs, with no evidence for a high-energy cutoff in the *BeppoSAX* range (up to ~100 keV).

In this paper, we report the results of a spectral study of a long (~200 ks) *BeppoSAX* observation of GX 349+2 in the energy range 0.1–200 keV. We find that, although the spectrum below 30 keV is similar to that observed during the observation reported on Paper I, the hard component is not present (or significantly weaker) during our observation, demonstrating that these hard tails can be highly variable and are probably not univocally related to the position in the CD.

2. OBSERVATIONS

The narrow-field instruments (NFIs) on board the *BeppoSAX* satellite are four coaligned instruments that cover more than three decades in energy, from 0.1 up to 200 keV, with good spectral resolution over the whole range (see Boella et al. 1997a for a detailed description of *BeppoSAX* instruments). These are two medium-energy concentrator spectrometers (MECSs; position-sensitive proportional counters operating in the 1.3–10 keV band; Boella et al. 1997b), a low-energy concentrator spectrometer (LECS; a thin-window, position-sensitive proportional counter with extended low-energy response, 0.1–10 keV; Parmar et al. 1997), a high-pressure gas scintillation proportional counter (HPGSPC; energy range of 7–60 keV; Manzo et al. 1997) and a phoswich detection system (PDS; energy range of 13–200 keV; Frontera et al. 1997).

In this paper, we report on two *BeppoSAX* observations of GX 349+2. The source was observed from 2001 February 12 11:23 UT to 2001 February 13 17:43 UT and from 2001 February 17 16:15 UT to 2001 February 19 20:42 UT. The total effective exposure times are ~30 ks for the LECS, ~138 ks for the MECS, ~130 ks for the HPGSPC, and ~66 ks for the PDS. We selected the data for the spectral analysis in circular regions centered on the source with $8'$ and $4'$ radii for LECS and MECS, respectively. The background subtraction was obtained with standard methods by using blank-sky observations. The background subtraction for the high-energy (nonimaging) instruments was obtained by using off-source data for the PDS and Earth occultation data for the HPGSPC.

In Figures 1 and 2 (*lower panels*), we show the 200 s binned MECS light curve of GX 349+2 in the 1.8–10.5 keV range for the first and the second observations, respectively; the light curve presents a large variability and the count rate varies from 130 up to 260 counts s^{-1}. In the upper and middle panels, we plot the soft color (SC), i.e., the ratio of the counts in the 4.5–7 to the 1.8–4.5 keV bands and the hard color (HC), i.e., the ratio of the counts in the 7–10.5 to the 4.5–7 keV energy bands, as functions of time.

In Figure 3, we show the CD of GX 349+2, where the HC and the SC are as defined above. The red triangles and the black stars indicate the positions of the source in the CD during a previous *BeppoSAX* observation taken in 2000 March (see Paper I) and during our observations, respectively. From this figure, it is clear that the position in the Z track was approximately the same during all the observations. To study the spectral variability along the CD, we selected five regions: SC < 0.47 (interval 1), 0.47 < SC < 0.50 (interval 2), 0.50 < SC < 0.55 (interval 3), 0.55 < SC < 0.60 (interval 4), and SC > 0.64 (interval 5), from which we extracted the corresponding count spectra.

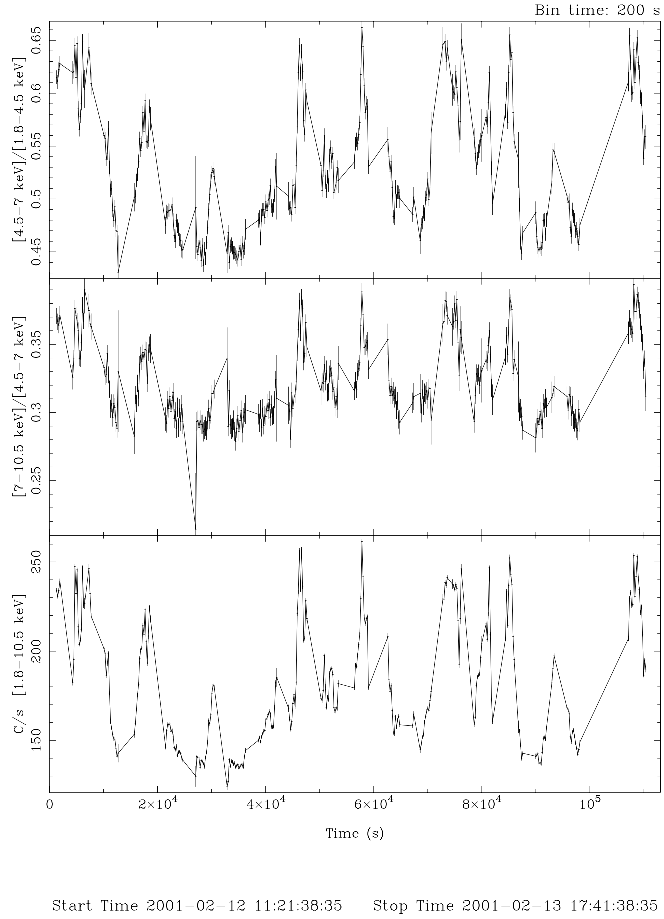

FIG. 1.—Soft color (*upper panel*), hard color (*middle panel*), and source count rate (*lower panel*) vs. time during the first part of the *BeppoSAX* observation of GX 349+2.

In Figure 4, we show the hardness-intensity diagram (HID), where the color on the *y*-axis is the SC and the intensity is the count rate of the source in the energy band 1.8–10.5 keV. The SC is a linear function of the intensity. We fitted the points using a linear relation $y = mx + q$, obtaining as best fit $m = (1.65 \pm 0.02) \times 10^{-3}$ and $q = 0.235 \pm 0.004$. This allows us to associate the corresponding count rate to the regions selected in the CD. In Table 1, we report the exposure times of the four instruments for each selected region and the corresponding count rate.

3. SPECTRAL ANALYSIS

We extracted an averaged spectrum from the whole observation, which is discussed in § 3.1. In § 3.2, we present the results obtained from the spectra selected in different regions of the CD. Relative normalizations of the four NFIs were treated as free parameters in model fitting, except for the MECS normalization, which was fixed to a reference value of 1. We checked after the fitting procedure that these normalizations were in the standard range for each instrument.[6] The energy ranges used in the spectral analysis were 0.12–3.5 keV for the LECS, 1.8–10 keV for the MECS, 7–30 keV for the HPGSPC, and 15–200 keV for the PDS. We rebinned the energy spectra in order to have approximately the same number of bins per instrument resolution element across the entire energy range. A 1% systematic error was applied to the spectra selected in different regions of the CD, and a 2% systematic error was applied to the averaged spectrum to take into account possible variability of the spectrum during the observation.

3.1. *The Averaged Spectrum*

We extracted an averaged spectrum from the two *BeppoSAX* observations. Following the results of Paper I, we started fitting the continuum with a blackbody plus a Comptonized component (Comptt; Titarchuk 1994) obtaining a χ^2 (dof) of 309 (197). In the residuals with respect to this model (see Fig. 5, *middle panel*) we find the presence of a weak hard excess at energies higher than 35 keV. Evident localized excesses are also present around 1.2, 2.6, and 6.7 keV, and an absorption feature is present between 9 and 10 keV.

The fit can be significantly improved by the addition of the components described below. We added a power-law component with photon index of 1.52 to fit the hard excess; an *F*-test gives a probability of chance improvement of the fit for the addition of this component of 1.9×10^{-7}. We added an absorption edge to fit the feature between 9 and 10 keV; the energy of the absorption edge is $\sim$9 keV, and its optical depth is $\tau \sim 3 \times 10^{-2}$. To fit the localized excesses, we used three narrow Gaussian emission lines. Initially we added a Gaussian line with its centroid at 1.18 keV and equivalent width $\sim$13 eV: its addition gave a probability of chance improvement of

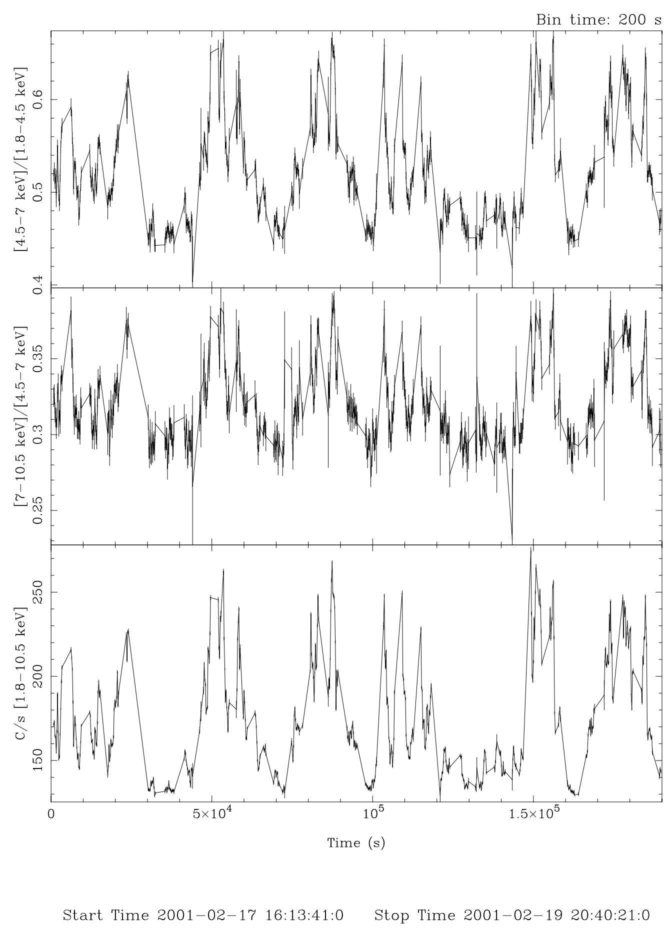

FIG. 2.—Soft color (*upper panel*), hard color (*middle panel*), and source count rate (*lower panel*) vs. time during the second part of the *BeppoSAX* observation of GX 349+2.

[6] See the *BeppoSAX* handbook at http://www.sdc.asi.it/software/index.html.

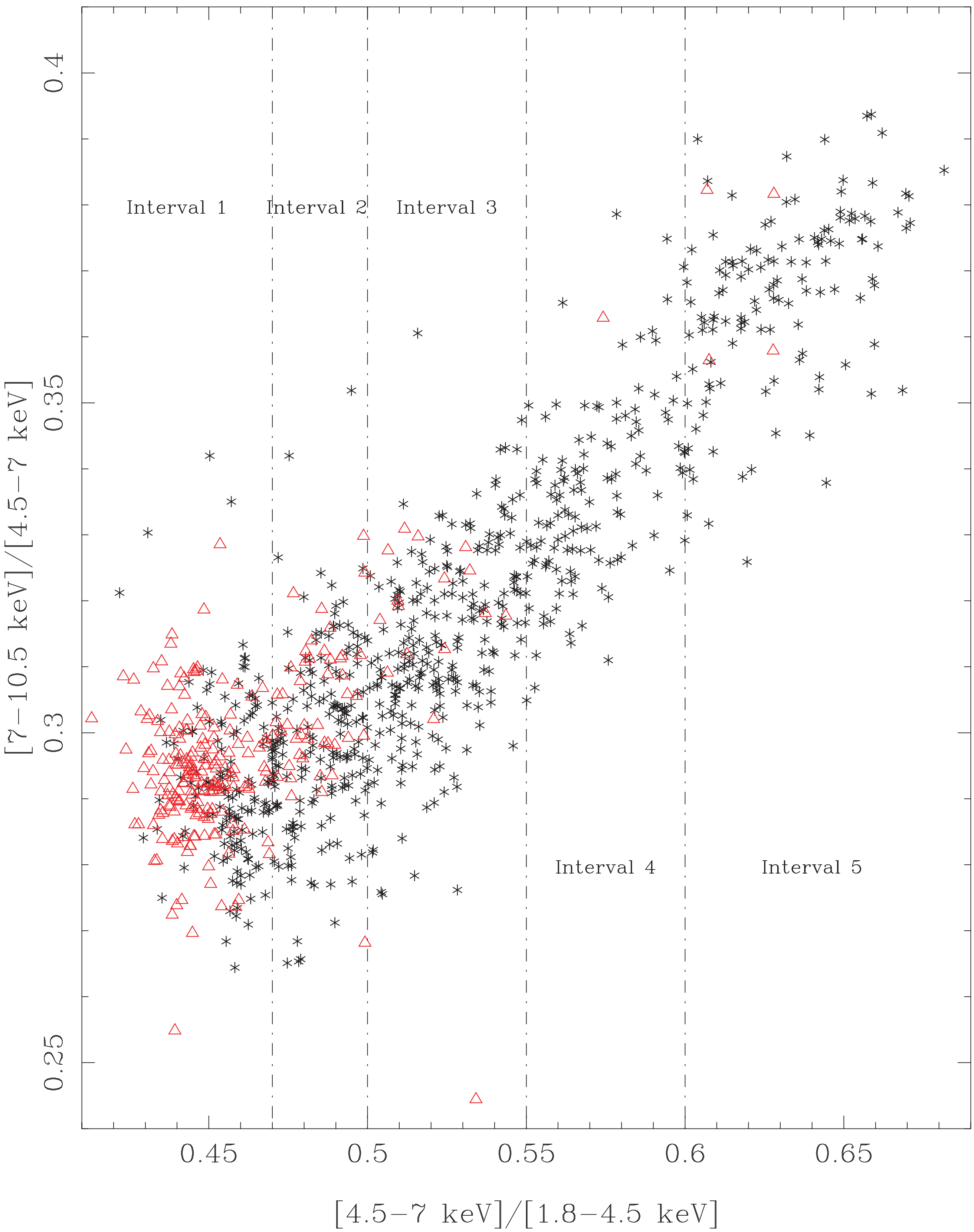

Fig. 3.—Color-color diagram of GX 349+2. Each bin corresponds to 200 s. The red triangles and the black stars indicate the position of the source obtained from the observation showed in Paper I and from our observations, respectively. The intervals, in which the CD is divided, are indicated by the dot-dashed vertical lines.

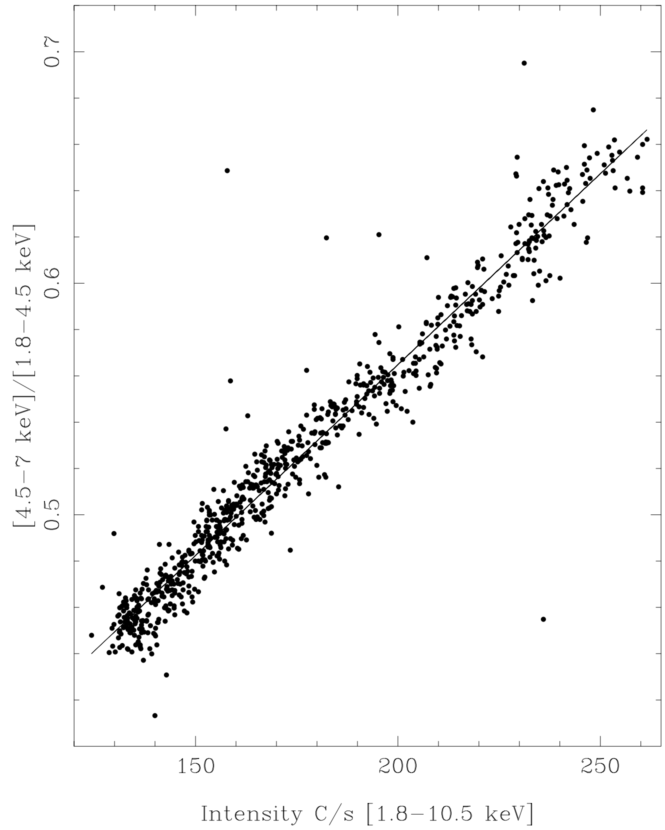

FIG. 4.—Hardness-intensity diagram of GX 349+2. Each bin corresponds to 200 s. *Solid line*: Best fit to the data using a linear relation $y = 1.65 \times 10^{-3}x + 0.235$.

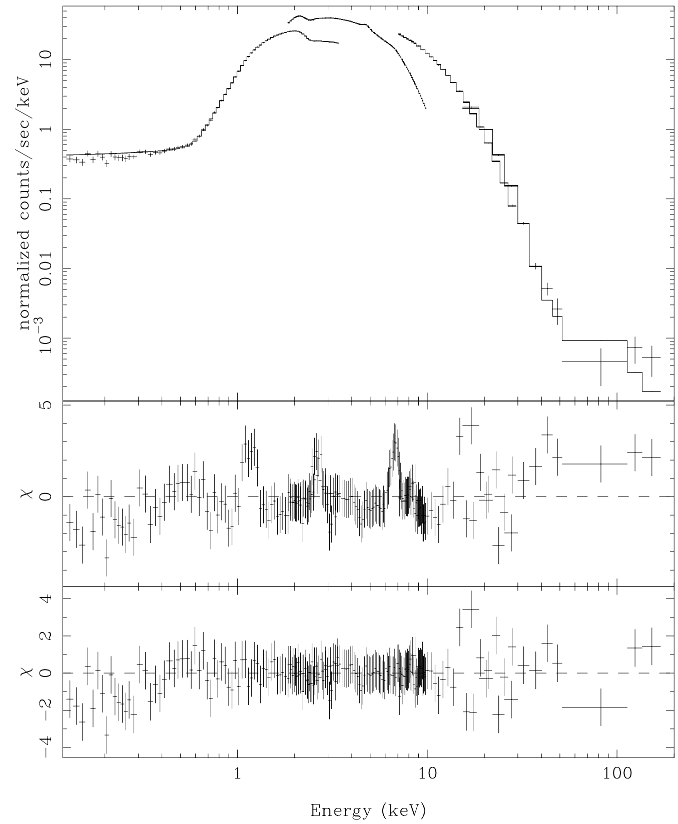

FIG. 5.—*Upper panel*: Averaged spectrum of GX 349+2 shown together with the best-fit model. *Middle panel*: Residuals in units of σ with respect to a simple model consisting of blackbody plus Comptt; three narrow features at 1.2, 2.6, and 6.7 keV, an absorption feature at around 9 keV, and a hard excess above 30 keV are present. *Lower panel*: Residuals in unit of σ with respect to the best-fit model.

1.1×10^{-8}. Then we added a Gaussian line with its centroid at 2.6 keV and equivalent width $\sim$10 eV: its addition gave a probability of chance improvement of $\sim 2.1 \times 10^{-5}$. Finally we added a Gaussian line with its centroid at 6.75 keV and equivalent width $\sim$39 eV: its addition gave a probability of chance improvement of $\sim 1.6 \times 10^{-9}$. The χ^2 (dof) of the best-fit model is 149 (184).

In Figure 5 (*upper and lower panels*), we plot the data and the residuals corresponding to the best-fit model described above, and in Figure 6, we plot the corresponding unfolded spectrum. In Tables 2 and 3, we report the parameters of the continuum and of the narrow features, respectively. The flux of the blackbody and of the Comptonized component in the energy band 0.1–200 keV are 0.45×10^{-8} and $\sim 2 \times 10^{-8}$ ergs cm^{-2} s^{-1}, respectively. The flux of the power-law component in the energy band 10–60 keV is $\sim 2.2 \times 10^{-11}$ ergs cm^{-2} s^{-1}, approximately 1 order of magnitude lower than the hard power-law flux during the observation reported on Paper I.

3.2. *Spectral Analysis as a Function of the Source Position in the CD*

We fitted the five spectra extracted from different positions in the source CD (see Fig. 3) using the model adopted for the averaged spectrum, keeping the photon index of the power-

TABLE 1

COUNT RATES AND EXPOSURE TIMES DURING THE *BeppoSAX* OBSERVATION OF GX 349+2

Intervals (1)	Counts s^{-1} (1.8–10.5 keV) (2)	LECS (ks) (3)	MECS (ks) (4)	HP (ks) (5)	PDS (ks) (6)
1..........................	133.0 ± 9.0	5	28	26	13
2..........................	152.0 ± 9.0	5	30	27	14
3..........................	176 ± 15	8	38	35	18
4..........................	206 ± 15	7	22	19	10
5..........................	242 ± 21	5	18	16	8
Total		30	136	123	63

NOTES.—In col. (2), we report the count rate of GX 349+2 corresponding to each selected region. The exposure times are shown in cols. (3), (4), (5), and (6) for each of the *BeppoSAX* NFIs, respectively. In line 6, we show the total exposure time for each NFI.

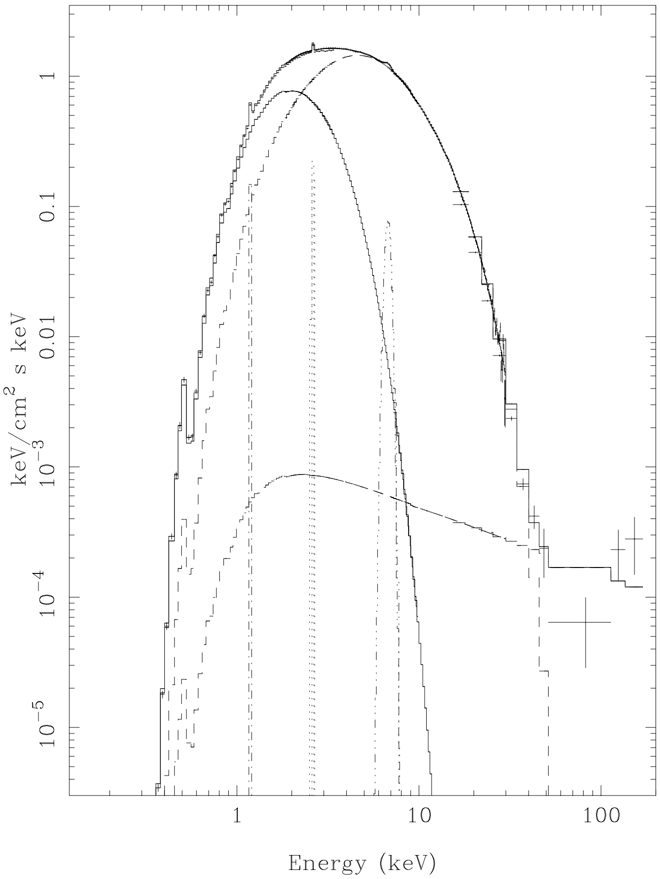

FIG. 6.—Unfolded averaged spectrum of GX 349+2 and the best-fit model indicated by the solid line on top of the data. The individual model components are also shown, namely the blackbody (*solid line*), the Comptonized spectrum (Comptt model; *dashed line*), three Gaussian emission lines at ∼1.2, ∼2.6, and ∼6.7 keV, and the hard power law (*dashed line*).

law component fixed at 1.52, the value obtained from the fit of the averaged spectrum. This model gives an acceptable fit for all the spectra. In Tables 4 and 5, we report the parameters of the continuum and of the narrow features for each spectrum. Going from interval 1 to interval 5, i.e., going to a higher intensity of the source, the flux of the blackbody component increases from 0.39×10^{-8} to 0.50×10^{-8} ergs cm^{-2} s^{-1} and the flux of the Comptonized component increases from $\sim 1.45 \times 10^{-8}$ to $\sim 3.0 \times 10^{-8}$ ergs cm^{-2} s^{-1}; the temperatures of the blackbody and of the Comptonized components also increase. In Figure 7, we show the fluxes and the temperatures of the blackbody and Comptonized components as a function of the count rate.

The addition of the Gaussian line at 1.18 keV is statistically significant in intervals 1, 2, and 3, and its equivalent width varies between 12 and 20 eV. The addition of the Gaussian line at 2.6 keV is significant in intervals 1, 2, 3, and 4, and its equivalent width is 8 eV. The addition of the Gaussian line at 6.7 keV is statistically significant in each interval, and its equivalent width decreases from 80 to 18 eV, going from interval 1 to interval 5. The decrease of the equivalent width is due to both an increase of the continuum flux and a decrease of the line intensity. The addition of an absorption edge at ∼9 keV, with an optical depth of ∼0.03, is always statistically significant. The addition of the power-law component is significant in interval 1 and interval 3, and the flux, in the energy band 10–60 keV, is between 1.4×10^{-11} and 2.8×10^{-11} ergs

TABLE 2

BEST-FIT PARAMETERS OF THE CONTINUUM EMISSION OF GX 349+2

Continuum Parameter	Value
N_H ($\times 10^{22}$ cm^{-2})	$0.673^{+0.048}_{-0.013}$
kT_{BB} (keV)	0.546 ± 0.016
N_{BB} ($\times 10^{-2}$)	$5.38^{+0.23}_{-0.25}$
R_{BB} (km)	35 ± 3
Flux$_{BB}$ ($\times 10^{-8}$ ergs cm^{-2} s^{-1})	0.45 ± 0.02
kT_0 (keV)	$1.197^{+0.033}_{-0.038}$
kT_e (keV)	$2.832^{+0.036}_{-0.050}$
τ	$11.06^{+0.40}_{-0.33}$
N_{Comptt}	$1.259^{+0.039}_{-0.031}$
Flux$_{Comptt}$ ($\times 10^{-8}$ ergs cm^{-2} s^{-1})	∼1.98
R_W (km)	7.6 ± 0.5
Photon Index	$1.52^{+1.57}_{-0.98}$
Power-law N ($\times 10^{-3}$)	$1.6^{+20.2}_{-1.6}$
Flux$_{po}$ (10–60 keV) ($\times 10^{-11}$ ergs cm^{-2} s^{-1})	2.3 ± 0.8
Chance Impr. Prob. Power Law	1.9×10^{-7}
χ^2_ν (dof)	0.81 (184)

NOTES.—Obtained from the averaged spectrum in the 0.12–200 keV energy band. The continuum consists of a blackbody, a Comptonized spectrum modeled by Comptt, and a power law. The notations kT_{BB} and N_{BB} are, respectively, the blackbody temperature and normalization in units of L_{39}/D_{10}, where L_{39} is the luminosity in units of 10^{39} ergs s^{-1} and D_{10} is the distance in units of 10 kpc. The notation kT_0 is the temperature of the seed photons for the Comptonization, kT_e is the electron temperature, τ is the optical depth of the scattering cloud using a spherical geometry, N_{Comptt} is the normalization of the Comptt model in XSPEC ver. 11 units, R_W is the Wien radius of the seed photons in km, and Flux$_{Comptt}$ is the bolometric flux corresponding to the Comptonization model in units of ergs cm^{-2} s^{-1}. The power-law normalization is in units of photons keV^{-1} cm^{-2} s^{-1} at 1 keV, and its flux is indicated as Flux$_{po}$. Uncertainties are at 90% confidence level for a single parameter of interest, the uncertainty on the power-law flux, Flux$_{po}$, is at 1 σ confidence level.

TABLE 3

BEST-FIT PARAMETERS OF THE DISCRETE FEATURES IN GX 349+2

Discrete Features Parameter	Value
E_{edge} (keV)	$9.09^{+0.59}_{-0.52}$
τ_{edge} ($\times 10^{-2}$)	$2.73^{+1.52}_{-1.36}$
E_{Fe} (keV)	$6.750^{+0.092}_{-0.095}$
σ_{Fe} (keV)	0.24 ± 0.16
I_{Fe} ($\times 10^{-3}$ photons cm^{-2} s^{-1})	$7.0^{+2.8}_{-2.1}$
Fe Equivalent Width (eV)	39 ± 13
Chance Impr. Prob. I_{Fe}	1.6×10^{-9}
$E_{1.2}$ (keV)	1.181 ± 0.027
$\sigma_{1.2}$ (keV)	< 0.08
$I_{1.2}$ ($\times 10^{-2}$ photons cm^{-2} s^{-1})	$1.49^{+0.70}_{-0.36}$
Emission–Line Equivalent Width (eV)	13^{+6}_{-3}
Chance Impr. Prob. $I_{1.2}$	1.1×10^{-8}
$E_{2.6}$ (keV)	2.595 ± 0.055
$\sigma_{2.6}$ (keV)	< 0.13
$I_{2.6}$ ($\times 10^{-3}$ photons cm^{-2} s^{-1})	$6.7^{+3.0}_{-2.4}$
Emission–line Equivalent Width (eV)	10 ± 4
Chance Impr. Prob. $I_{2.6}$	2.1×10^{-5}

NOTES.—Obtained from the averaged spectrum. Three Gaussian emission lines and an absorption edge are detected. The centroids, widths, and normalizations of the lines are indicated respectively by E, σ, and I. The labels 1.2, 2.6, and Fe correspond to the lines at 1.2, 2.6, and 6.7 keV, respectively. Uncertainties are at 90% confidence level for a single parameter of interest.

TABLE 4
THE 0.12–200 keV CONTINUUM BEST-FIT PARAMETERS OF GX 349+2

Continuum Parameter	Interval 1	Interval 2	Interval 3	Interval 4	Interval 5
$N_H (\times 10^{22}$ cm$^{-2})$	$0.666^{+0.027}_{-0.024}$	$0.671^{+0.025}_{-0.020}$	$0.664^{+0.016}_{-0.015}$	$0.686^{+0.038}_{-0.017}$	$0.683^{+0.025}_{-0.019}$
kT_{BB} (keV)	$0.508^{+0.011}_{-0.018}$	$0.526^{+0.011}_{-0.018}$	0.537 ± 0.012	$0.549^{+0.012}_{-0.007}$	0.568 ± 0.013
N_{BB} $(\times 10^{-2})$	$4.60^{+0.28}_{-0.21}$	$5.06^{+0.13}_{-0.19}$	$5.21^{+0.15}_{-0.16}$	5.73 ± 0.18	5.97 ± 0.18
R_{BB} (km)	37 ± 3	36 ± 3	36 ± 2	35 ± 2	34 ± 2
Flux$_{BB}$ $(\times 10^{-8}$ ergs cm^{-2} s$^{-1})$	0.39 ± 0.02	0.42 ± 0.01	0.44 ± 0.01	0.48 ± 0.02	0.50 ± 0.02
kT_0 (keV)	$1.030^{+0.042}_{-0.039}$	$1.119^{+0.021}_{-0.032}$	$1.176^{+0.024}_{-0.026}$	$1.238^{+0.026}_{-0.025}$	1.298 ± 0.029
kT_e (keV)	2.722 ± 0.042	$2.807^{+0.040}_{-0.047}$	2.784 ± 0.034	$2.810^{+0.033}_{-0.047}$	2.811 ± 0.042
τ	$11.24^{+0.36}_{-0.34}$	$10.58^{+0.36}_{-0.28}$	$11.04^{+0.30}_{-0.28}$	$11.55^{+0.33}_{-0.31}$	12.35 ± 0.34
N_{Comptt}	$1.031^{+0.049}_{-0.043}$	$1.085^{+0.044}_{-0.037}$	1.271 ± 0.037	$1.542^{+0.042}_{-0.037}$	$1.783^{+0.039}_{-0.040}$
Flux$_{Comptt}$$(\times 10^{-8}$ ergs cm^{-2} s$^{-1})$	~ 1.45	~ 1.64	~ 1.94	~ 2.48	~ 3.00
R_W (km)	8.9 ± 0.7	8.8 ± 0.7	7.9 ± 0.4	7.8 ± 0.4	7.4 ± 0.4
Photon Index	1.52 (fixed)	1.52 (fixed)	1.52 (fixed)	1.52 (fixed)	1.52 (fixed)
Power-Law N $(\times 10^{-3})$	2.02 ± 1.04	1.21 ± 1.10	$2.23^{+0.77}_{-1.08}$	< 1.27	1.83 ± 1.40
Flux$_{po}$ (10–60 keV) $(\times 10^{-11}$ ergs cm^{-2} s$^{-1})$	~ 2.8	~ 1.7	~ 3.1	< 1.4	~ 2.5
Chance Impr. Prob. Power Law	2.5×10^{-3}	0.20	9.4×10^{-4}	0.13	0.06
χ^2_ν (dof)	1.06 (184)	1.26 (183)	1.24 (184)	1.29 (186)	1.14 (187)

NOTES.—Obtained from the spectra extracted in different positions in the CD. The parameters are defined as in Table 2. Uncertainties are at 90% confidence level for a single parameter of interest, except that the uncertainty of Flux$_{po}$ is at 1 σ.

cm^{-2} s^{-1}, as reported in Table 4, similar to the value found for the averaged spectrum.

4. DISCUSSION

We studied the *BeppoSAX* energy spectra of GX 349+2, extracted at different positions of the source in the CD. The best-fit model up to energies of $\sim$30 keV consists of a blackbody and a Comptonization spectrum (described by the Comptt model), three emission lines, and an absorption edge.

The equivalent hydrogen column, N_H, derived from the best-fit model is $\sim 0.67 \times 10^{22}$ cm^{-2}, in agreement with the results of Paper I. Cooke & Ponman (1991), using data from the medium- and low-energy X-ray detectors on *EXOSAT*, obtained a value of $(0.86 \pm 0.01) \times 10^{22}$ cm^{-2} and evaluated the visual extinction in the direction of the source to be $A_V = 3.9 \pm 0.5$ mag; a similar value of $\sim 0.8 \times 10^{22}$ cm^{-2}, which implies a distance to GX 349+2 of 5 kpc, was reported by Christian & Swank (1997) using the *Einstein* solid state spectrometer (SSS; 0.5–4.5 keV). Using the value of the equivalent hydrogen column to the source that we obtain from the *BeppoSAX* observations, we can recalculate the visual extinction from the observed correlation between visual extinction and absorption column (Predehl & Schmitt, 1995); this gives $A_V \simeq 3.6-4.1$ mag, still compatible with the values previously reported (Cooke & Ponman 1991; Penninx & Augusteijn 1991). In the direction of GX 349+2, this would correspond to a distance between 3.6 and 4.4 kpc

TABLE 5
BEST-FIT PARAMETERS OF THE DISCRETE FEATURES OF GX 349+2

Discrete Features Parameter	Interval 1	Interval 2	Interval 3	Interval 4	Interval 5
E_{edge} (keV)	9.15 ± 0.19	$8.98^{+0.29}_{-0.26}$	$9.05^{+0.42}_{-0.25}$	$9.53^{+0.20}_{-0.15}$	9.43 ± 0.30
$\tau_{edge}$$(\times 10^{-2})$	4.8 ± 1.3	$3.7^{+1.7}_{-1.2}$	3.4 ± 1.0	$3.9^{+1.3}_{-1.2}$	3.8 ± 1.1
E_{Fe} (keV)	$6.710^{+0.055}_{-0.060}$	6.735 ± 0.039	6.746 ± 0.053	6.765 ± 0.068	6.711 ± 0.094
σ_{Fe} (keV)	$0.39^{+0.10}_{-0.09}$	0.208 ± 0.075	$0.244^{+0.082}_{-0.073}$	< 0.30	< 0.29
$I_{Fe}$$(\times 10^{-3}$ photons cm^{-2} s$^{-1})$	$9.2^{+2.2}_{-1.6}$	$7.6^{+1.4}_{-1.3}$	$7.2^{+1.6}_{-1.3}$	$6.3^{+1.8}_{-1.5}$	$4.9^{+1.9}_{-1.7}$
Fe Equivalent Width (eV)	77 ± 15	52 ± 11	40 ± 8	28 ± 8	18 ± 7
Chance Impr. Prob. I_{Fe}	~ 0	~ 0	~ 0	2.2×10^{-10}	1.2×10^{-5}
$E_{1.2}$ (keV)	1.180 (fixed)	1.181 ± 0.027	$1.190^{+0.030}_{-0.036}$	$1.15^{+0.10}_{-0.22}$	$1.21^{+0.06}_{-0.14}$
$\sigma_{1.2}$ (keV)	< 0.23	< 0.08	< 0.08	< 0.29	< 0.20
$I_{1.2}$ $(\times 10^{-2}$ photons cm^{-2} s$^{-1})$	$2.1^{+4.3}_{-0.9}$	$2.6^{+1.0}_{-0.8}$	$1.42^{+0.70}_{-0.49}$	$1.1^{+4.8}_{-0.6}$	$1.1^{+1.3}_{-0.7}$
Emission–line Equivalent Width (eV)	20^{+38}_{-9}	23 ± 8	13 ± 6	9^{+40}_{-5}	9^{+11}_{-6}
Chance Impr. Prob. $I_{1.2}$	2.0×10^{-4}	9.4×10^{-7}	5.0×10^{-4}	0.11	0.11
$E_{2.6}$ (keV)	2.629 ± 0.070	$2.613^{+0.038}_{-0.059}$	$2.622^{+0.059}_{-0.064}$	$2.636^{+0.050}_{-0.056}$	$2.620^{+0.070}_{-0.074}$
$\sigma_{2.6}$ (keV)	< 0.32	< 0.12	< 0.12	< 0.10	< 0.13
$I_{2.6}$ $(\times 10^{-3}$ photons cm^{-2} s$^{-1})$	$4.7^{+3.0}_{-2.1}$	$4.6^{+2.7}_{-0.9}$	$5.2^{+2.3}_{-1.9}$	$6.0^{+2.4}_{-2.0}$	$4.8^{+2.6}_{-2.4}$
Emission-Line Equivalent Width (eV)	8 ± 4	7^{+4}_{-1}	7^{+4}_{-2}	8 ± 3	6 ± 3
Chance Impr. Prob. $I_{2.6}$	7.9×10^{-3}	4.5×10^{-3}	2.0×10^{-3}	1.8×10^{-3}	0.04

NOTES.—Obtained from the spectra extracted in different positions in the CD. The parameters are defined as in Table 3. Uncertainties are at 90% confidence level for a single parameter of interest.

(Hakkila et al. 1997). These values are not very different from 5 kpc. Therefore, we will continue to adopt 5 kpc for the distance to GX 349+2 to facilitate the comparison with previous results. Note, however, that all the luminosities quoted here can be lower by a factor of ~1.3–1.9.

The blackbody temperature is $kT_{\rm BB} \sim 0.5 - 0.6$ keV, its luminosity, in the energy range 0.1–200 keV, is $\sim 1.34 \times 10^{37}$ ergs s^{-1}, and the radius of the blackbody emitting region is $R_{\rm BB} \sim 36$ km. The blackbody temperature and flux both increase with an increase in the source luminosity (see Fig. 7), while the blackbody radius does not significantly change. The luminosity of the Comptonized component, in the 0.1–200 keV band, is $\sim 3.4 \times 10^{37}$ ergs s^{-1}, 80% of the total luminosity, and is ~20% of the Eddington luminosity for a 1.4 $M_\odot$ NS. The temperature of the soft-seed photons for the Comptonization is $kT_0 \sim 1$ keV. These are Comptonized in a hotter ($kT_e \sim 3$ keV) region of moderate optical depth ($\tau = 10-12$ for a spherical geometry). The radius of the region emitting the seed-photon Wien spectrum, calculated as in In 't Zand et al. (1999), is $R_{\rm W} = 3 \times 10^4 D\left[{\rm Flux_{Comptt}}/(1+y)\right]^{1/2}/(kT_0)^2$ km = 7–9 km, where D is the distance in kpc, ${\rm Flux_{Comptt}}$ is the bolometric flux of the Comptonization component in ergs cm^{-2} s^{-1}, y is the Compton parameter, and kT_0 is in keV. We note that $R_{\rm W}$ is comparable with the radius of a NS. The seed photon temperature significantly increases with the source luminosity (see Fig. 7). There is small evidence of an increase of the optical depth and a decrease of the radius of the seed photon–emitting region with increasing source luminosity, while the electron temperature is consistent with being constant.

A broad (~0.7 keV FWHM) iron K-shell emission line is present at ~6.7 keV, with equivalent width between 18 and 85 eV, which decreases with increasing the source luminosity. This is accompanied by an absorption edge at ~9 keV, with an optical depth of $\tau \sim 0.04$. The high energy of both the iron line and edge indicates that these features are produced in a highly ionized region (corresponding approximately to Fe xxv). We also found evidence for an emission line at ~1.2 keV, with equivalent width of 9–20 eV, slightly decreasing with increasing source luminosity, which can be associated with emission from the L shell of Fe xxiv (see, e.g., Kallman et al. 1996) and an emission line at 2.6 keV, with an equivalent width of 10 eV, which can be associated with Lyα emission from S xvi.

The ionization parameters, $\log_{10}\xi$, corresponding to S xvi, Fe xxiv, and Fe xxv are 3.1, 3.04, and 3.67, respectively. From $\xi = L_x/n_e r^2$ (see Krolik, McKee, & Tarter 1981) and $L_{\rm line} = 4\pi D^2 I_{\rm line} = n_e^2 V \alpha A f$, we can obtain the distance, r, from the central source and the corresponding densities of the region where the lines are produced. In these formulas, $L_{\rm X}$ is the total X-ray luminosity of the source in the energy band 0.1–200 keV, n_e the electron density, $L_{\rm line}$ the luminosity of the line, D the distance to the source, $I_{\rm line}$ the intensity of the line, V the emitting volume, α the recombination parameter, A the cosmic abundance of the element, and f the fractional number of ions in the given ionization state of the considered element. We assumed a spherical volume of radius r and fixed $f = 1$. The recombination parameter α was obtained using the relation and the best-fit parameters for S xvi, Fe xxiv, and Fe xxv reported by Verner & Ferland (1996), where we fixed the plasma temperature at the electron temperature of the Comptonizing cloud. For the averaged spectrum, we find that the Fe xxv line is produced at $r = 5.1 \times 10^9$ cm, with a corresponding electron density of $n_e = 5.9 \times 10^{14}$ cm^{-3}, the S xvi line at $r = 1.0 \times 10^{10}$ cm with $n_e = 5.7 \times 10^{14}$ cm^{-3}, and finally, the Fe xxiv line at $r = 2.6 \times 10^{10}$ cm with $n_e = 9.2 \times 10^{13}$ cm^{-3}. On the other hand, if we assume that the Comptonizing cloud is indeed an accretion disk corona (ADC), where the coronal temperature is the electron temperature of the cloud, then the coronal radius is $R_c \sim M_{\rm NS}/M_\odot\, T_7^{-1}\, R_\odot$ (White & Holt 1982), where $M_{\rm NS}$ is the NS mass and T_7 the coronal temperature in units of 10^7 K. Assuming a NS mass of 1.4 $M_\odot$ and the electron temperature obtained from the fit, we find $R_c \sim 3 \times 10^{10}$ cm. This implies that the Fe xxv line is produced at $r \sim 0.17R_c$, the S xvi line at $r \sim 0.34R_c$, and the Fe xxiv line at $r \sim 0.87R_c$. The Fe xxv line is broader than the S xvi and Fe xxiv lines, probably because it is produced in the inner region of the corona, and the escaping photons are more effected by Compton scattering.

A weak narrow absorption feature is present at ~4.2 keV. We fitted this component using an absorption edge and found an upper limit of the optical depth of $\tau \sim 3.82 \times 10^{-2}$. This absorption edge could correspond to the K edge of Ar xvii, dominating at an ionization parameter of $\log_{10}\xi \sim 3$. The corresponding Ar xvii emission line should be found at ~3.14 keV. Supposing that it is produced in the same region as Fe xxiv, that is the external region of the corona, and using the parameters of density and radius obtained for Fe xxiv, the cosmic abundance of Ar and the corresponding recombination parameter (Verner & Ferland 1996), we obtain an intensity of the Ar xvii line of $\sim 1.1 \times 10^{-3}$ photons cm^{-2} s^{-1}; from the fit, we find a compatible upper limit of the intensity of $\sim 2 \times 10^{-3}$ photons cm^{-2} s^{-1}, implying that the Ar xvii line may be overwhelmed by the continuum emission.

We repeated the same procedure for the spectra extracted in the different region of the CD in order to study the emission

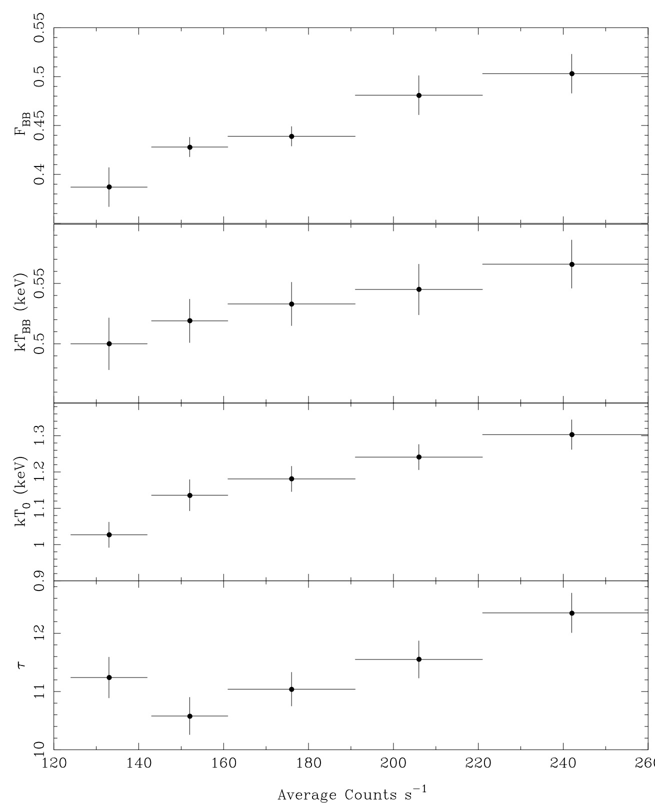

Fig. 7.—Evolution of the spectral parameters as a function of the source luminosity/position in the CD. *From top to bottom*: Blackbody flux in units of 10^{-8} ergs cm^{-2} s^{-1}, blackbody temperature in keV, seed-photon temperature in keV, and optical depth of the Comptonizing cloud.

TABLE 6

RADIUS IN CM AND ELECTRON DENSITY IN CM^{-3} OF THE REGION IN WHICH EMISSION LINES ARE PRODUCED

Line	Interval 1	Interval 2	Interval 3	Interval 4	Interval 5
S XVI	$r = 8.6 \times 10^9$	$r = 1.1 \times 10^{10}$	$r = 1.3 \times 10^{10}$	$r = 1.7 \times 10^{10}$	...
	$n_e = 5.9 \times 10^{14}$	$n_e = 4.4 \times 10^{14}$	$n_e = 3.5 \times 10^{14}$	$n_e = 2.5 \times 10^{14}$	...
Fe XXIV	$r = 1.1 \times 10^{10}$	$r = 1.1 \times 10^{10}$	$r = 2.7 \times 10^{10}$	...	...
	$n_e = 4.4 \times 10^{14}$	$n_e = 4.9 \times 10^{14}$	$n_e = 9.0 \times 10^{13}$	...	...
Fe XXV	$r = 2.3 \times 10^9$	$r = 3.4 \times 10^9$	$r = 4.8 \times 10^9$	$r = 9.5 \times 10^9$	$r = 1.5 \times 10^{10}$
	$n_e = 2.2 \times 10^{15}$	$n_e = 1.2 \times 10^{15}$	$n_e = 6.5 \times 10^{14}$	$n_e = 2.6 \times 10^{14}$	$n_e = 9.8 \times 10^{13}$

region of the lines at different source luminosities; the results, for the statistically significant lines, are reported in Table 6. It is evident that when the count rate increases, the formation region of the lines moves to larger radii where the density is lower.

One of the main results of this paper regards the hard component. At energies higher than 30 keV, a hard excess is indeed present in our observations. However, the 10–60 keV flux of the power-law component that we used to fit this hard excess is 1 order of magnitude lower than that measured during the *BeppoSAX* observation of 2000 March (Paper I), although the source was in a similar position of the Z track. In Paper I, a hard component was required to match the spectrum above 30 keV during the nonflaring emission. This component could be fitted by a power law with photon index ~ 2 and with a flux of 1.2×10^{-10} ergs cm^{-2} s^{-1} in the energy range 10–60 keV. In our observations, the photon index of the power law is 1.5 (still compatible with the previous value), while the flux in the same energy band is $\sim 2 \times 10^{-11}$ ergs cm^{-2} s^{-1}. Indeed, we cannot exclude that the power law we fitted during our observations is due to the hard diffuse emission of the Galactic ridge. Using data from Valinia & Marshall (1998), for latitudes $1\overset{\circ}{.}5 < |b| < 4^\circ$ and longitudes $|l| < 15^\circ$ (the region of GX 349+2), the flux of the diffuse Galactic emission is $\sim 3.2 \times 10^{-11}$ ergs cm^{-2} s^{-1} in the 10–60 keV energy range for the effective solid angle of the PDS FOV, and the photon index of the power law is 1.7 ± 0.2. These values are compatible to those we found in our analysis of GX 349+2. We conclude that the hard power-law component during these new *BeppoSAX* observations is much weaker or even absent.

A hard power-law component was observed in several Z sources, indicating that this is probably a common feature of these sources. The presence (or strength) of these components appears sometimes to be related to the source state or its position in the CD. The only clear example of this behavior was given by a *BeppoSAX* observation of GX 17+2. In this source, the intensity of the hard component (a power law with a photon index of ~ 2.7) showed the strongest intensity in the HB of its CD; a factor of ~ 20 decrease was observed when the source moved from the HB to the NB, i.e., from a low to a high inferred mass accretion rate. For other sources, some evidence was found that the hard component becomes weaker for higher accretion rates (GX 5−1, Asai et al. 1994; GX 349+2, Paper I; Cyg X-2, Di Salvo et al. 2002; Cir X-1, Iaria et al. 2001). However, in recent *RXTE*/HEXTE observations of Sco X-1, a hard power-law tail was detected in five out of 16 observations, without any clear correlation with the position in the CD (D'Amico et al. 2001). GX 349+2 may show a behavior that is similar to the one observed in Sco X-1. Indeed GX 349+2, as well as GX 17+2, is classified as a Sco-like source, which are thought to have a lower inclination than the other Z sources (referred to as Cyg-like sources; Kuulkers et al. 1994; Kuulkers & van der Klis 1995), and similarly to Sco X-1 (but not to GX 17+2), does spend a relatively short time in the HB (i.e., at the lowest inferred mass accretion rates).

The behavior of Sco X-1 and GX 349+2 suggests that there might be a second parameter, besides mass accretion rate or position of the source in the Z track, regulating the presence of hard emission in these systems. As already mentioned, the second parameter regulating the spectral state transitions might be the truncation radius of the optically thick disk. However, what determines the radius at which the disk is truncated is not clear yet: this could be the mass accretion rate through the disk normalized by its own long-term average (as proposed by van der Klis 2001), but also magnetic fields, the fraction of power dissipated in a hot, optically thin, corona (see, e.g., Chen 1995), or the formation/quenching of a jet could play a role. Interestingly, Strickman & Barret (2000) suggest that the hard X-ray emission present in Sco X-1 data from OSSE may be correlated with periods of radio flaring.

This might be generally true for these kinds of systems. Although the mass accretion rate appears to be the main parameter driving the spectral hardness of atoll sources, there is evidence that at least on occasions an additional parameter controls the soft/hard spectral transitions. A clear example is given by a recent observation of 4U 1705−44, in which the source underwent a soft- to hard-state transition while the 0.1–200 keV bolometric luminosity of the source decreased by a factor of ~ 3 from the soft to the hard state and increased by only a factor of ~ 1.2 in the opposite transition from the hard to the soft state (Barret & Olive 2002). On another occasion, the same source displayed hard and soft states in which the source luminosity was different by a much larger factor, up to 1 order of magnitude. Again, the second parameter regulating the spectral state transitions might be the truncation radius of the optically thick disk. Note also that even though variations of the mass accretion rate appear to be the main cause of the spectral transitions of accreting black hole candidates (BHCs), there is some evidence that a second, yet unknown, parameter can give rise to these transitions. The existence of a second parameter was indeed proposed to explain the soft/hard spectral transitions observed in the BHCs XTE J1550−564 (Homan et al. 2001) and GS 2000+25 (Tanaka 1989).

There might be, however, another explanation for the difference in the hard X-ray component between the 2000 March and the 2001 February *BeppoSAX* observations. From the light curves shown in Figures 1 and 2 it is clear that the source was continuously flaring during the last *BeppoSAX* observation. The longest continuous time interval that the source spent in a persistent flux level (below ~ 200 counts s^{-1}) is ~ 25 ks. On the other hand, the source spent a longer continuous time in a persistent flux level during the previous observation, showing only one large (i.e., with a count rate higher than 200 counts s^{-1}) flare during almost 100 ks of total observation time (see a light curve in Fig. 1 of Paper I). It can therefore be that the continuous flaring activity during the last *BeppoSAX* observation has quenched the hard X-ray emission. In other words, while the source was mainly in the vertex between the NB and the FB (where the hard X-ray component was indeed significantly detected) during the previous *BeppoSAX* observation with only a short excursion into the FB, the source was mainly in the FB during the last *BeppoSAX* observation. In this case, the nondetection of the hard component during the last *BeppoSAX* observation is in agreement with the nondetection of the hard component during the flaring state in the previous *BeppoSAX* observation (although the relatively low statistics, because of the short exposure time, did not allow a definitive conclusion in the previous observation) and with the paradigm that the hard emission is suppressed at the highest inferred mass accretion rates.

This work was partially supported by the Italian Space Agency (ASI) and by the Ministero della Istruzione, della Università e della Ricerca (MIUR). T. D. acknowledges the Netherlands Organization for Scientific Research (NWO).

REFERENCES

Agrawal, P. C., et al. 1971, Ap&SS, 10, 500
Asai, K., et al. 1994, PASJ, 46, 479
Barret, D., & Olive, J. F. 2002, ApJ, 576, 391
Boella, G., Butler, R. C., Perola, G. C., Piro, L., Scarsi, L., & Blecker, J. 1997a, A&AS, 122, 299
Boella, G., et al. 1997b, A&AS, 122, 327
Chen, X. 1995, ApJ, 448, 803
Christian, D. J., & Swank, J. H. 1997, ApJS, 109, 177
Cooke, B. A., & Ponman, T. J. 1991, A&A, 244, 358
D'Amico, F., Heindl, W. A., Rothschild, R. E., & Gruber, D. E. 2001, ApJ, 547, L147
Di Salvo, T., & Stella, L. 2002, in Proc. XXII Moriond Astrophys. Meeting, The Gamma-Ray Universe, ed. A. Goldwurm, D. Neumann, & J. Tran Thanh Van (Hanoi: Thê Gioi), in press
Di Salvo, T., et al. 2000, ApJ, 544, L119
———. 2001, ApJ, 544, 49
———. 2002, A&A, 386, 535
Ford, E. C., et al. 1996, ApJ, 469, L37
Frontera, F., et al. 1997, A&AS, 122, 357
———. 1998, Nucl. Phys. B, 69, 286
Greenhill, J. G., Coe, M. J., Burnell, S. J. B., Strong, K. T., & Carpenter, G. F. 1979, MNRAS, 189, 563
Hakkila, J., et al. 1997, AJ, 114, 2043
Hasinger, G., & van der Klis, M. 1989, A&A, 225, 79
Hasinger, G., van der Klis, M., Ebisawa, K., Dotani, T., & Mitsuda, K. 1990, A&A, 235, 131
Haymes, R. C., Harnden, F. R., Johnson, W. N., Prichard, H. M., & Bosch, H. E. 1972, ApJ, 172, L47
Homan, J., et al. 2001, ApJS, 132, 377
Iaria, R., Burderi, L., Di Salvo, T., La Barbera, A., & Robba, N. R. 2001, ApJ, 547, 412
In't Zand, J. J. M., et al. 1999, A&A, 345, 100
Jain, A., et al., 1984, A&A, 140, 179
Kallman, T. R., Liedahl, D., Osterheld, A., Goldstein, W., & Kahn, S. 1996, ApJ, 465, 994
Krolik, J. H., McKee, C. F., & Tarter, C. B. 1981, ApJ, 249, 422
Kuulkers, E., & van der Klis, M. 1995, A&A, 303, 801
Kuulkers, E., et al. 1994, A&A, 289, 795
Manzo, G., Giarrusso, S., Santangelo, A., Ciralli, F., Fazio, G., Piraino, S., & Segreto, A. 1997, A&AS, 122, 341
Miyamoto, S., & Matsuoka, M. 1977, Space Sci. Rev., 20, 687
O'Neill, P. M., Kuulkers, E., Sood, R. K., Dotani, T. 2001, A&A, 370, 479
O'Neill, P. M., Kuulkers, E., Sood, R. K., & van der Klis, M. 2002, MNRAS, 336, 217
Parmar, A. N., et al. 1997, A&AS, 122, 309
Penninx, W., & Augusteijn, T. 1991, A&A, 246, L81
Peterson, L. E. 1973, in IAU Symp. 55, X- and Gamma-Ray Astronomy, ed. H. Bradt & R. Giacconi (San Francisco: ASP), 51
Peterson, L. E., & Jacobson, A. S. 1966, ApJ, 145, 962
Piraino, S., Santangelo, A., Ford, E. C., & Kaaret, P. 1999, A&A, 349, L77
Predehl, P., & Schmitt, J. H. M. M. 1995, A&A, 293, 889
Riegler, G. R., Boldt, E., & Serlemitsos, P. 1970, Nature, 266, 1041
Soong, Y., & Rothschild, R. E. 1983, ApJ, 274, 327
Strickman, M., & Barret, D. 2000, in AIP Conf. Proc. 510, Detections of Multiple Hard X-Ray Flares from Sco X-1 with OSSE, ed. M. L. McConnel & J. M. Ryan (New York: AIP), 222
Tanaka, Y. 1989, in 23rd ESLAB Symp., Two Topics in X-Ray Astronomy, Vol. 1: X Ray Binaries, ed. N. White (Noordwijk: ESA), 3
Titarchuk, L. 1994, ApJ, 434, 570
Ubertini, P., Bazzano, A., Cocchi, M., La Padula, C., & Sood, R. K. 1992, ApJ, 386, 710
Valinia, A., & Marshall, F. E. 1998, ApJ, 505, 134
van der Klis, M. 1995, X-Ray Binaries (Cambridge: Cambridge Univ. Press), 252
———. 2000, ARA&A, 38, 717
———. 2001, ApJ, 561, 943
Verner, D. A., & Ferland, G. J. 1996, ApJS, 103, 467
White, N. E., & Holt, S. S. 1982, ApJ, 257, 318
Zhang, W., Strohmayer, T. E., & Swank, J. H. 1998, ApJ, 500, L167